metals

MDPI

Article

Viscous Flow Properties and Structural Evolution of Vanadium-Containing Hot Metal: Experiments and Molecular Dynamics Simulation

Jiawei Chen [1], Yufei Pan [1], Penghui Guo [1,*], Xinyi Li [1], Zhuogang Pang [1], Zhenghua Shen [1], Shan Ren [2], Donghui Wei [1,*] and Xiangdong Xing [1,*]

[1] School of Metallurgical Engineering, Xi'an University of Architecture and Technology, Xi'an 710055, China; cjw0311@xauat.edu.cn (J.C.); panyufei@xauat.edu.cn (Y.P.); lixiny@xauat.edu.cn (X.L.)
[2] School of Energy and Power Engineering, Xi'an Jiaotong University, Xi'an 710049, China
* Correspondence: guoph@xauat.edu.cn (P.G.); weidh@xauat.edu.cn (D.W.); xaxxd@xauat.edu.cn (X.X.)

Abstract

To reveal the effect of vanadium content on the viscous flow behavior of vanadium-containing hot metal, viscosity measurements and molecular dynamics simulations were conducted. The viscosity and melting characteristic temperature were measured. The local structures of Fe, V, and C atoms were analyzed using radial distribution functions, average coordination numbers, mean square displacements, and cluster evolution. Both viscosity and melting characteristic temperature increased with vanadium content. At 1300 °C, the viscosity increased from 11.8 to 19.9 mPa·s as the vanadium content increased from 0.20 to 0.30 wt%. The melting characteristic temperature increased from 1242 to 1323 °C. Structural analysis showed that increasing vanadium content promoted the redistribution of C atoms. The average coordination number of V–C increased from 7.780 to 8.218. In contrast, the coordination numbers of C–Fe and Fe–C decreased. The mean square displacements of Fe and C atoms also decreased, indicating that atomic diffusion was suppressed. Cluster evolution further showed that V–C structures could dissociate and recombine with Fe–C and Fe–V units. Therefore, increasing vanadium content reduced the fluidity of hot metal by increasing the melting characteristic temperature, strengthening V–C local coordination, and promoting complex cluster formation.

Keywords: vanadium-containing hot metal; viscosity; structure; molecular dynamics simulation; vanadium–titanium magnetite

Check for updates

Academic Editor: Changming Fang

Received: 26 July 2026
Revised: 13 August 2026
Accepted: 16 August 2026
Published: 19 August 2026

Copyright: © 2026 by the authors. Licensee MDPI, Basel, Switzerland. This article is an open access article distributed under the terms and conditions of the Creative Commons Attribution (CC BY) license.

1. Introduction

Vanadium–titanium magnetite is a polymetallic mineral in which iron, vanadium, and titanium coexist. In addition to serving as an iron feedstock for blast furnace smelting, it is an important source of the strategic metals vanadium and titanium [1–3]. China has abundant and widely distributed reserves of vanadium–titanium magnetite. In addition to the proven deposits in the Panxi and Chengde regions, such mineral resources are also found in northwestern regions such as Hami and Bachu in Xinjiang [3]. The efficient development and utilization of such ore deposits can enhance the region's resource security and reduce the country's reliance on imported iron ore. Compared with conventional hot metal, hot metal produced from vanadium–titanium magnetite contains appreciable vanadium and exhibits more complex physicochemical and flow behavior [4]. During the production of high-vanadium hot metal, variations in vanadium content can alter

the local melt structure and interactions among constituent elements, thereby affecting fluidity. These changes directly influence tapping stability, slag-metal separation, and coordination with downstream steelmaking operations [5,6]. Therefore, understanding the mechanisms by which vanadium content affects the fluidity of molten iron is crucial for the efficient smelting of vanadium–titanium magnetite and the stable production of high-vanadium molten iron.

Viscosity is a key property governing hot-metal fluidity because it reflects the internal friction opposing flow [7]. Previous studies have examined the viscosity of conventional hot metal and vanadium- and titanium-containing hot metal [8–10]. Deng et al. [6], for example, used the oscillating crucible method to measure hot metal viscosity over a range of temperatures and compositions and evaluated the effects of temperature and elemental content. Hou et al. [11] investigated how vanadium content affects the formation of high-melting phases and their relationship with the viscosity of hot metal produced from vanadium–titanium magnetite. These studies established composition–viscosity relationships through macroscopic measurements and phase analysis. An atomistic assessment of how vanadium content alters local structure, atomic coordination, and diffusion is still required to explain the microscopic origin of the observed viscosity changes.

With advances in computational materials science, molecular dynamics (MD) simulation has become an important tool for investigating the local structure and atomic behavior of metallic melts [12,13]. Yan et al. [14] used MD simulations to determine the effects of carbon content on the density, viscosity, and self-diffusion coefficients of molten iron, revealing systematic composition- and temperature-dependent changes in its thermophysical properties. Shen et al. [4] showed that Ti–C coordination, increasingly complex cluster structures, and suppressed atomic diffusion were associated with higher viscosity in titanium-containing hot metal. These studies demonstrate that MD simulations can resolve local coordination and atomic transport in molten iron and thus provide a suitable basis for examining how vanadium modifies hot metal viscosity. However, previous studies have mainly focused on conventional Fe–C melts or others hot metal. The atomic-scale response of vanadium-containing hot metal to variations in vanadium content remains insufficiently understood. In particular, the coupled evolution of viscosity, characteristic melting temperature, V–C local coordination, atomic mobility, and multicomponent Fe–V–C cluster structures remains understood. Therefore, the present study bridges macroscopic flow behavior with atomic scale structural evolution by combining viscosity measurements with molecular dynamics simulations over a controlled range of vanadium contents.

In this study, viscosity measurements were combined with MD simulations to determine the effects of vanadium content and temperature on the viscosity of vanadium-containing hot metal. Atomic coordination, local cluster structures, and diffusion behavior were analyzed to establish the relationship between viscosity and atomic-scale structural evolution. These findings provide useful guidance for optimizing vanadium content and temperature control in industrial vanadium–titanium magnetite smelting. They also provide a mechanistic basis for understanding and controlling the fluidity of vanadium-containing hot metal.

2. Materials and Methods

2.1. Experimental Materials

The pig iron used in the experiments was obtained from an operating steel plant in China. Ferrovanadium alloy was added to adjust the vanadium content of the hot metal. The compositions of the pig iron and ferrovanadium alloy are shown in Table 1.

Table 1. Components of pig iron and high purity titanium (wt%).

Material	C	Si	Mn	S	P	V	Ti	Fe
Pig iron	4.391	0.256	0.232	0.062	0.067	0.113	0.124	94.755
Ferrovandium alloy	0.035	0.920	0.057	0.018	0.028	80.30	-	18.642

2.2. Experimental Procedure

2.2.1. Premelting of Hot Metal

Surface oxides and adhering impurities were removed from the pig iron samples before weighing. The required mass of ferrovanadium alloy was calculated from the target vanadium content and weighed accordingly. The pig iron and ferrovanadium alloy were then placed together in an alumina crucible (Sinopharm Chemical Reagent Co., Ltd., Shanghai, China), heated to 1500 °C at 5 °C·min^{-1} under argon, and held for 30 min to ensure complete melting and homogenization. After premelting, the samples were immediately water-quenched and dried. Their compositions are shown in Table 2. After premelting, the chemical compositions of the samples were analyzed using an X-ray fluorescence spectrometer (XRF, PANalytical B.V., Almelo, The Netherlands). Before analysis, the surface oxide layer was removed and the sample surface was ground to obtain a clean and flat analytical surface.

Table 2. Composition of premelted sample (wt%).

Sample	C	Si	Mn	S	P	V	Ti
V1	4.391	0.256	0.232	0.062	0.067	0.113	0.124
V2	4.389	0.256	0.232	0.062	0.067	0.150	0.124
V3	4.386	0.257	0.232	0.062	0.067	0.200	0.124
V4	4.384	0.257	0.232	0.062	0.067	0.250	0.124
V5	4.381	0.258	0.232	0.062	0.067	0.300	0.124
V6	4.378	0.258	0.231	0.062	0.067	0.350	0.124
V7	4.375	0.258	0.231	0.062	0.067	0.400	0.124
V8	4.373	0.259	0.231	0.062	0.067	0.450	0.124
V9	4.370	0.259	0.231	0.062	0.067	0.500	0.124

2.2.2. Measurement of Viscosity and Characteristic Melting Temperature

Hot metal viscosity was measured using an RTW-10 melt physical properties analyzer (Northeastern University, Shenyang, China) in the rotating-cylinder mode. Surface oxides and impurities were removed from each premelted sample before it was loaded in a corundum crucible. The sample was raised to a temperature of 1500 °C in the viscometer and held for 30 min. Viscosity was then measured during stepwise cooling, with a 30 min holding period at each target temperature before data acquisition. The rotational oscillation of the molten hot metal in the corundum crucible was recorded as a decay curve, and viscosity was calculated from the relationship between the logarithmic decrement of the rotational oscillation and melt viscosity. The characteristic melting temperature was determined using the procedure commonly applied to slags and was defined as the temperature at which the slope of the viscosity-temperature curve equaled −1. Before each high-temperature viscosity measurement, the viscometer was calibrated using castor oil to ensure measurement accuracy. For each composition, the viscosity measurement was independently repeated three times under identical experimental conditions, and the average value of the three measurements was reported. The standard deviation of the three measurements was calculated to evaluate experimental repeatability.

2.2.3. Molecular Dynamics Simulations

(1) Simulation parameters

All molecular dynamics simulations were performed using the open source Large-scale Atomic/Molecular Massively Parallel Simulator (LAMMPS, 2 August 2023). To describe the many-body interactions associated with metallic bonding in Fe-based melts and the local electron-density variations introduced by alloying elements. The atomic interactions in the present simulations were described within the EAM framework [15,16]. In this method, the total potential energy is decomposed into the energy required to embed an atom in the surrounding electron density and the pairwise interaction energy, as expressed by Equation (1) [15]:

$$U(\{r_{ab}\}) = \sum_{a,b>a} V^{(X_a,X_a)}(r_{ab}) + \sum_{a} F^{(X_a)}(\rho_a) \quad (1)$$

$$\rho_a = \sum_{a \neq b} \Phi^{(X_a,X_a)}(r_{ab}) \quad (2)$$

where E is the total potential energy of the system; $F_i(\rho_i)$ is the embedding energy of atom i in the local electron density ρ_i; $\varphi_{ij}(r_{ij})$ is the pair-interaction term between atoms i and j; r_{ij} is the interatomic distance; and $f_j(r_{ij})$ represents the contribution of atom j to the electron density at atomic site i X represents atomic species.

The chemical compositions of the simulation systems were based on the measured compositions of the premelted samples. The mass fractions of C, Si, Mn, S, P, and Ti were held constant, while the V mass fraction was set to 0.10, 0.20, 0.30, 0.40, or 0.50 wt.%, with the balance assigned to Fe (Table 3). Each model set contained 10,000 atoms; the mass fractions of each element were first converted to atomic fractions, and the corresponding number of atoms was then determined based on these values. Minor deviations resulting from rounding were compensated for by adjusting the number of Fe atoms to ensure that the total number of atoms was consistent across different models.

Table 3. Simulation calculation of hot metal composition (wt%).

Sample ID	C	Si	Mn	S	P	V	Ti
M1	4.39	0.25	0.23	0.06	0.07	0.10	0.10
M2	4.39	0.25	0.23	0.06	0.07	0.20	0.10
M3	4.39	0.25	0.23	0.06	0.07	0.30	0.10
M4	4.39	0.25	0.23	0.06	0.07	0.40	0.10
M5	4.39	0.25	0.23	0.06	0.07	0.50	0.10

(2) Simulation procedure

A cubic simulation box was constructed based on the initial density of a body-centered cubic Fe crystal, and atoms were randomly introduced into the simulation box according to Table 3 to obtain initial configurations with different vanadium contents. The x, y and z axes were all imposed with periodic boundary conditions to reduce the influences of free surfaces and finite simulation sizes. Temperature and pressure were controlled using the Nosé–Hoover method, and the atomic truncation distance was set to 10.3 Å.

Before starting the calculation, the conjugate gradient method was used to eliminate any excessively close atomic contacts that might exist in the initial model and to reduce the system's potential energy. Subsequently, the atoms were supplied with initial velocities at 300 K according to the Maxwell–Boltzmann distribution and allowed to relax for 3 ns at that temperature. Under the NPT ensemble, the system was heated to 2500 K at 1000 K·ns^{-1} and equilibrated dynamically for another 3 ns to remove the structural memory of the

initial lattice and obtain a homogeneous liquid. The system was subsequently cooled to the target temperature and equilibrated for 0.5 ns, followed by a 1 ns production run during which atomic trajectories were recorded. These trajectories were used to calculate radial distribution functions (RDFs), average coordination numbers, and mean square displacements (MSDs). For each pair of atoms, the first minimum following the first peak of the radial distribution function was selected as the integration cutoff radius, thereby uniformly defining the first coordination sphere. The cutoff radii used to define the first coordination shell for the Fe–Fe, Fe–C, V–C, and V–Fe atomic pairs were 3.6, 4.0, 3.7, and 3.6 Å, respectively. These cutoff radii were subsequently used for the calculation of the corresponding coordination numbers.

The mean square displacement was calculated by time-averaging the squares of the displacements of each atom relative to its initial position and was used to characterize the mobility of iron, carbon, and other particles.

3. Results and Discussion

3.1. Viscosity and Melting Temperature

Figure 1 shows the viscosity and characteristic melting temperature of molten iron at different vanadium contents. As shown in Figure 1a, the viscosity of all alloys decreased with increasing temperature, indicating that heating improved melt flowability; viscosity increased with increasing vanadium content, and its dependence on temperature became significantly stronger. Between 0.10 and 0.25 wt.% V, the viscosities remained relatively low and differed only slightly. At 0.30 wt.% V and above, the viscosity increased markedly, particularly below 1400 °C. At 1300 °C, increasing the vanadium content from 0.25 to 0.30 wt.% raised the viscosity from 13.2 to 19.9 mPa·s, and the magnitude of the increase continued to grow at higher vanadium contents. With a further increase in V content to 0.35–0.50 wt.%, the viscosity continued to increase. These results indicate that the influence of vanadium on viscosity is relatively limited at low V contents but becomes increasingly significant once the V content approaches and exceeds approximately 0.30 wt.%.

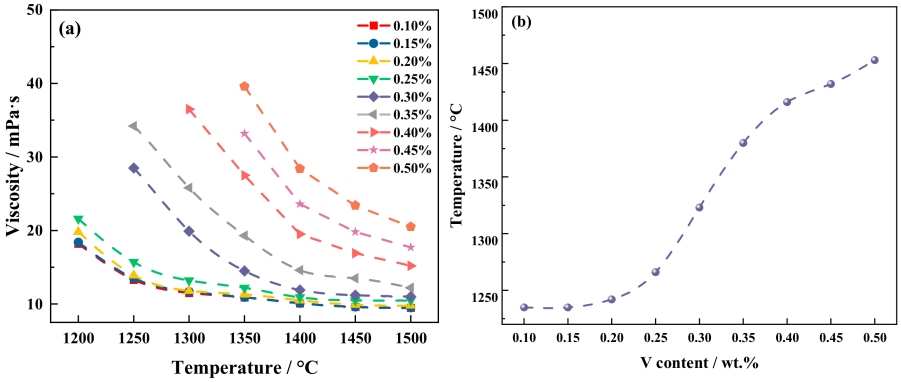


Figure 1. (**a**) Viscosity–temperature curves and (**b**) melting characteristic temperature curves of hot metal with different vanadium contents.

Figure 1b shows the characteristic melting temperatures of vanadium-containing molten iron. Overall, these temperatures increased with rising vanadium content, but the rate of increase varied across different composition ranges. Between 0.10 and 0.20 wt.% V, the characteristic melting temperature remained within 1235 to 1242 °C. It rose rapidly above 0.25 wt.% V. In particular, increasing the vanadium content from 0.25 to 0.35 wt.% raised the characteristic melting temperature from 1266 to 1380 °C, an increase of approximately 114 °C. At 0.40 wt.% V, the temperature increased further to approximately 1416 °C. With a further increase in V content, the characteristic melting temperature continued to

increase, reaching approximately 1416 °C at 0.40 wt.% V and approximately 1450 °C at 0.50 wt.% V. Vanadium therefore reduced hot-metal fluidity through concurrent increases in viscosity and characteristic melting temperature. The marked changes above 0.30 wt.% V suggested that this composition range represented a transition from relatively stable flow behavior to pronounced deterioration.

3.2. Molecular Dynamics Analysis

3.2.1. Effect of Vanadium Content on the Local Structure

Figure 2 presents the RDFs of Fe–C, Fe–Fe, V–C, C–C, and V–Fe atomic pairs in vanadium-bearing hot metal at 1500 °C. Figure 2a compares the atomic-pair RDFs for the M3 system. The nearest-neighbor distances, obtained from the positions of the first peaks, decreased in the order C–C > V–C > Fe–C > V–Fe > Fe–Fe. The shorter Fe–C distance relative to C–C indicated that the first coordination shell of C was dominated by Fe. Similarly, the shorter V–Fe distance relative to V–C showed that Fe atoms lay closer to V than C atoms. The distinct first peak of the V–C RDF nevertheless indicated a strong short-range association between V and C [17,18].

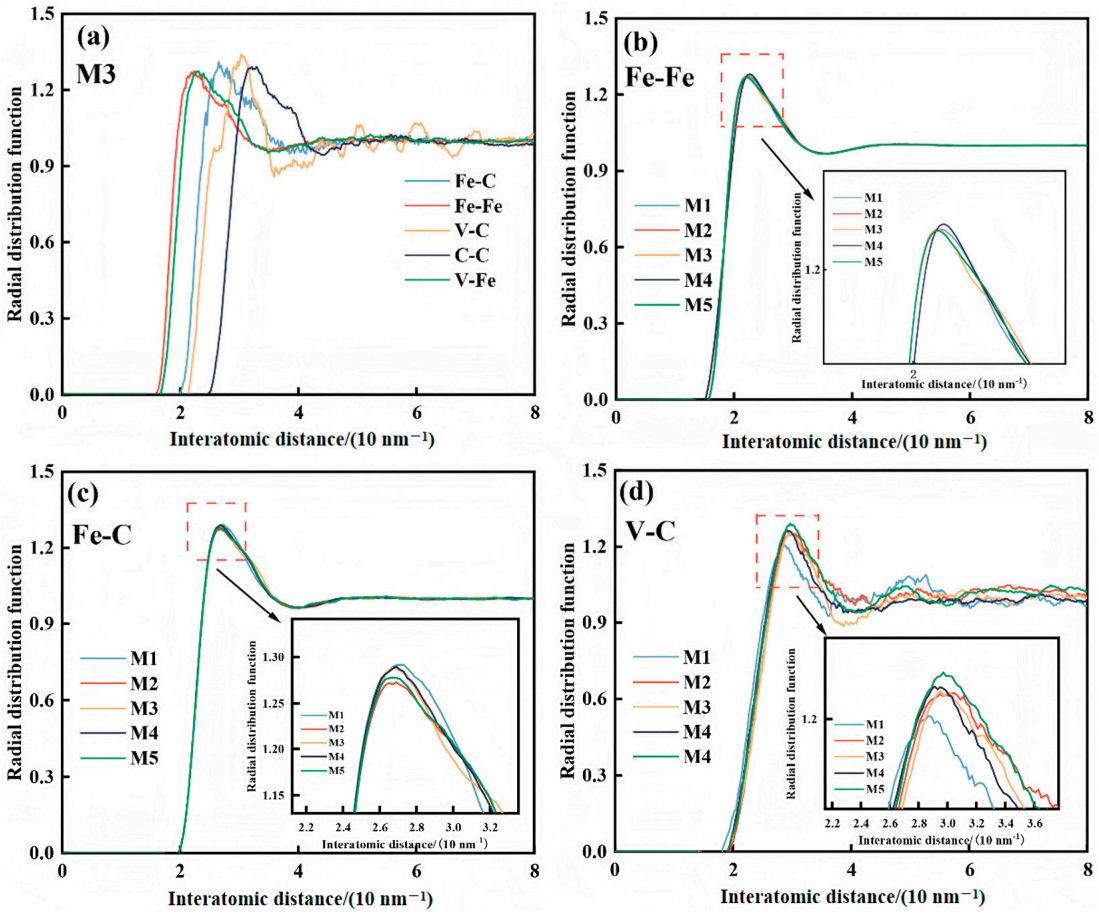


Figure 2. Radial distribution functions (RDFs) from molecular dynamics simulations for vanadium-containing hot metal. (**a**) Multiple atomic-pair RDFs of sample M3; (**b**) Fe–Fe RDFs; (**c**) Fe–C RDFs; (**d**) V–C RDFs.

The Fe–Fe RDFs at different vanadium contents are shown in Figure 2b. As the vanadium content increased from 0.10 to 0.50 wt.%, the curves remained nearly coincident. The first-peak position was essentially unchanged, and only small variations in peak height were observed. Vanadium content therefore had little effect on Fe–Fe pairs or the local arrangement of Fe, and the Fe-dominated short-range structure remained

stable [19]. Figure 2c shows the Fe–C RDFs. Their first peaks were located at approximately 2.71×10^{-1} nm and exhibited little variation in height, indicating that the local Fe coordination around C was also relatively insensitive to vanadium content [20]. In contrast, the V–C RDFs in Figure 2d changed systematically. As the vanadium content increased from 0.10 to 0.50 wt.%, the first V–C peak generally increased in height and shifted toward a larger interatomic distance. These changes indicated enhanced V–C short-range order and a more ordered local distribution of C around V.

Figure 3 depicts the average coordination numbers among Fe, V, and C at different vanadium contents. The average coordination number represented the number of neighboring atoms within the first coordination shell of a central atom and provided a measure of local structural order. At 0.10 wt.% V, the average number of Fe atoms around a central C atom (C–Fe) was 4.565, whereas the average number of C atoms around a central Fe atom (Fe–C) was 0.980. Thus, C was predominantly coordinated by Fe and participated in Fe–C short-range structures. The average number of C atoms around a central V atom (V–C) was 7.780, indicating a pronounced nearest-neighbor association between V and C and a tendency to form local clusters.

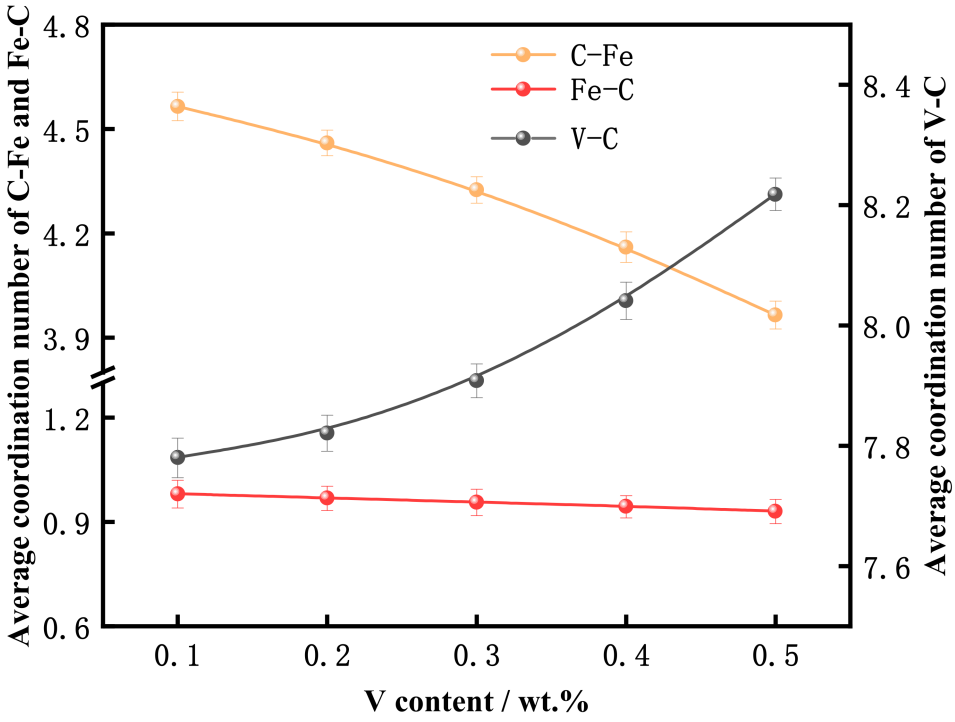


Figure 3. Effect of vanadium contents on the average coordination numbers of C–Fe, Fe–C, and V–C.

As the V mass fraction increased from 0.10 to 0.50 wt.%, the C–Fe coordination number decreased from 4.565 to 3.965 and the Fe–C coordination number decreased from 0.980 to 0.930. In contrast, the V–C coordination number increased from 7.780 to 8.218, indicating enhanced short-range order in the V–C system. The increase in the number of vanadium atoms promoted preferential coordination between vanadium and carbon, causing a redistribution of the local environment of some carbon atoms-shifting from iron-centered and carbon-centered Fe–C configurations to V–C configurations. The resulting increase in V–C connectivity was consistent with a more complex local melt structure and greater atomic migration resistance, which might be one of the reasons for the observed increase in viscosity.

The MSD characterizes atomic mobility in molten hot metal. Figure 4 demonstrates the MSDs of Fe and C at different vanadium contents [21–24]. At a given vanadium content,

the MSD of Fe was consistently higher than that of C, indicating greater Fe mobility. Both the MSD values and curve slopes of Fe and C decreased as the vanadium content increased, demonstrating suppressed atomic diffusion. The differences among the C curves were more pronounced, showing that vanadium had a stronger effect on C mobility. This behavior was consistent with enhanced local V–C coordination, which constrained C migration and stabilized the local melt structure [25,26]. At the common compositions of 0.20, 0.30, 0.40, and 0.50 wt.% V, the experimental results show an overall increase in viscosity and characteristic melting temperature with increasing V content. Correspondingly, the MD results show progressively enhanced V–C coordination and reduced Fe and C atomic mobility. These changes indicate that the deterioration in fluidity is accompanied by strengthened V–C local ordering and restricted atomic migration.

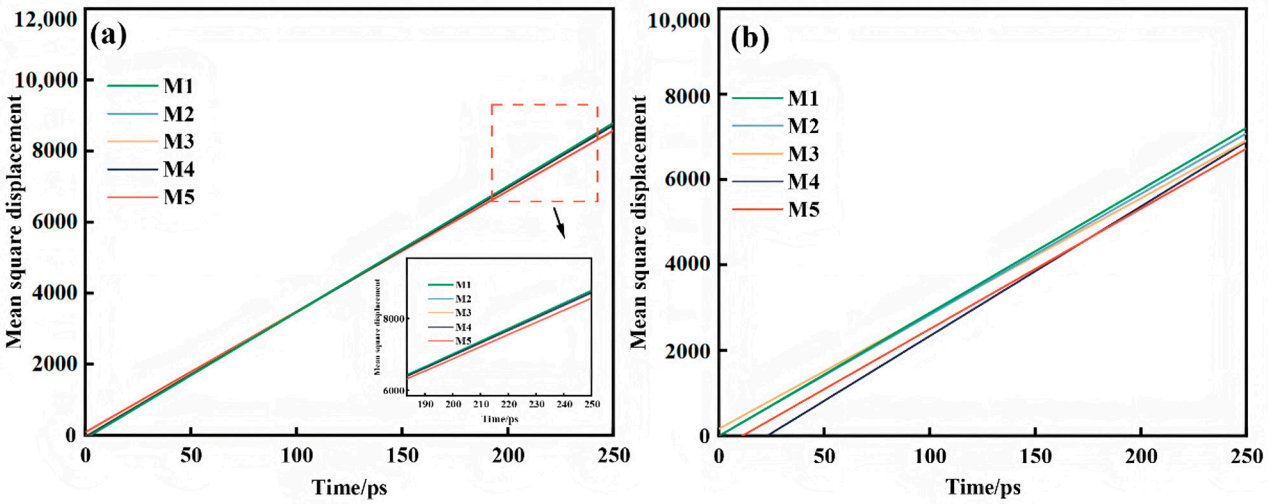


Figure 4. Effect of vanadium content on the mean square displacements (MSDs) of Fe and C atoms. (**a**) MSD curves of Fe atoms; (**b**) MSD curves of C atoms.

3.2.2. Temperature Dependent Evolution of Local Structures

Figure 5 shows the RDFs of Fe–Fe, Fe–C, V–Fe, and V–C pairs in vanadium-containing hot metal over 1200–1500 °C. The location of the primary peak for atomic pairs varied little with temperature, indicating that temperature had a minor effect on the nearest-neighbor distances between atoms, and that the nearest-neighbor structure of the major atomic pairs in the melt was relatively stable. As the temperature decreased, the peak heights of the first peaks for all atomic pairs generally increased, indicating that the local atomic arrangements became more compact and the local structure tended toward stability. Among these, the changes in the V–C atomic pair were most pronounced; the peak height of its first peak increased significantly with decreasing temperature, suggesting that cooling enhanced the short-range order between V and C, facilitating the formation of stable V–C local structural units and cluster structures.

The effect of temperature on the coordination structure of vanadium-containing hot metal is shown in Figure 6. When the temperature rose from 1200 to 1500 °C, the C–Fe coordination number decreased from approximately 4.552 to 4.156, while the Fe–C coordination number declined from 0.981 to 0.935. Heating therefore weakened local Fe–C coordination and promoted partial dissociation of Fe–C clusters. Over the same temperature range, the V–C coordination number decreased from approximately 8.033 to 7.882.

Figure 7 illustrates the effect of temperature on the MSDs of Fe and C. From 1200 to 1500 °C, both MSDs increased approximately linearly with time, and their slopes generally increased with temperature, indicating enhanced atomic mobility. The increase was most pronounced from 1200 to 1400 °C. The curves at 1400 and 1500 °C were comparatively close,

suggesting that the incremental effect of further heating on atomic diffusion diminished in the upper part of the investigated temperature range.

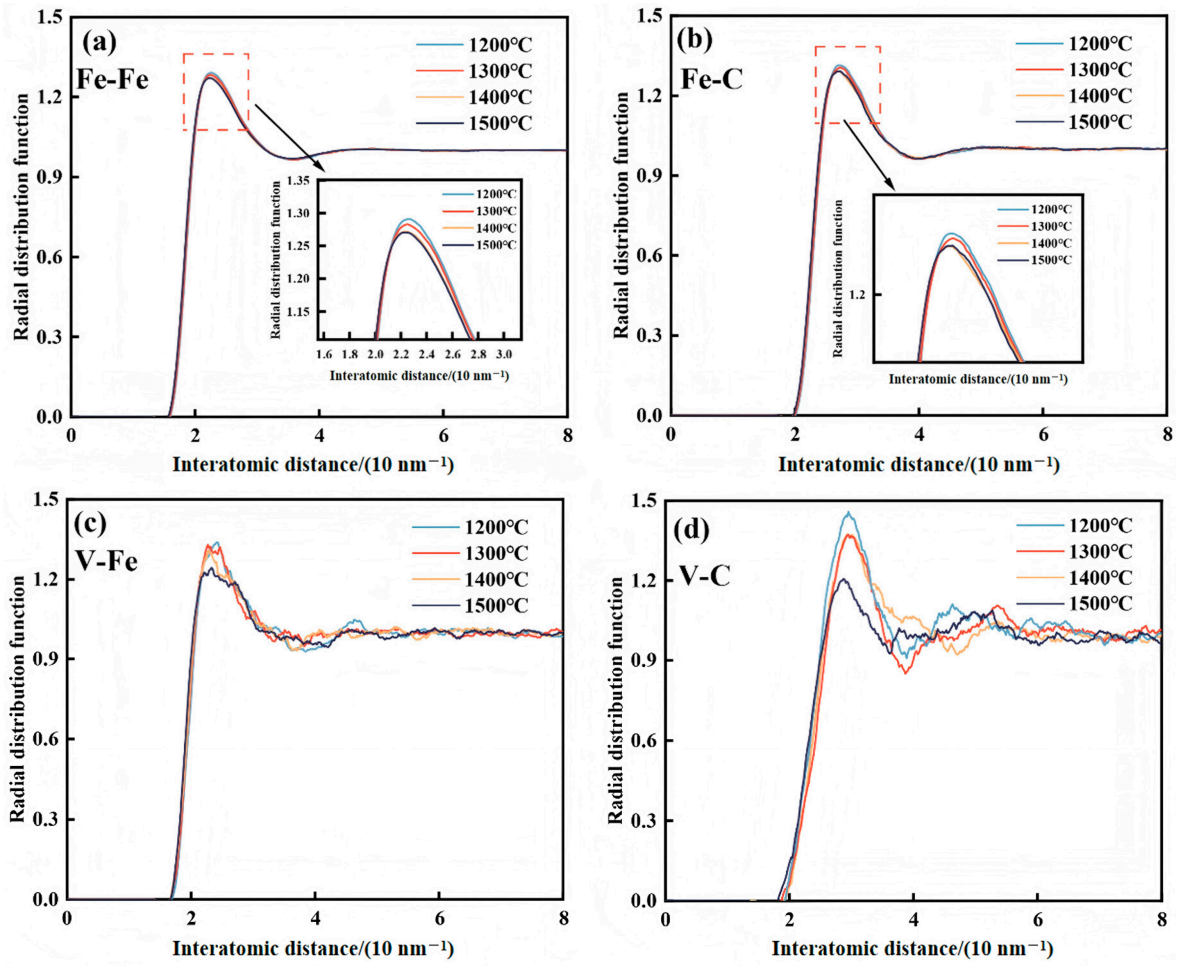


Figure 5. Effect of temperature on the radial distribution functions (RDFs) of vanadium-containing hot metal. (**a**) Fe–Fe RDFs; (**b**) Fe–C RDFs; (**c**) V–Fe RDFs; (**d**) V–C RDFs.

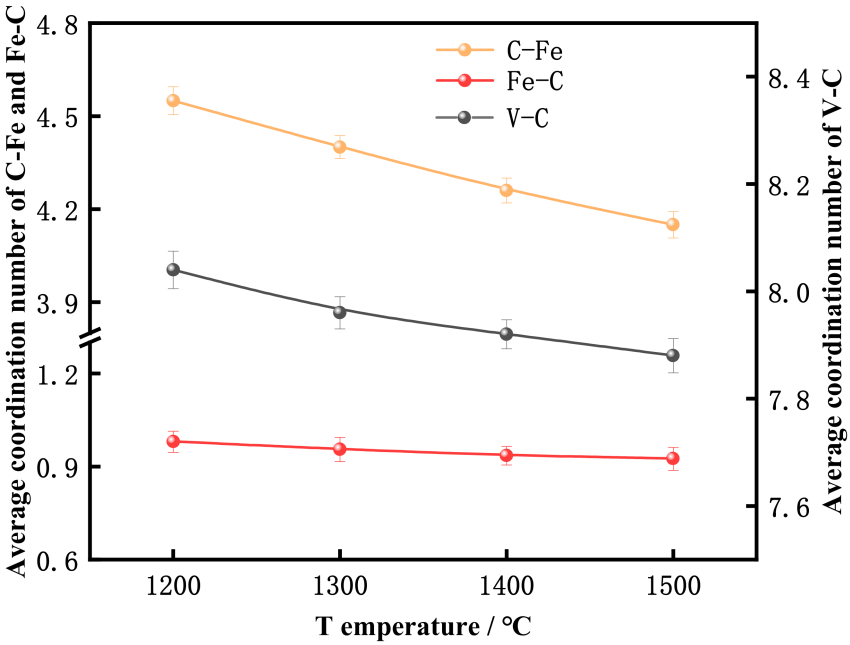


Figure 6. Effect of temperature on the coordination numbers of M3 hot metal.

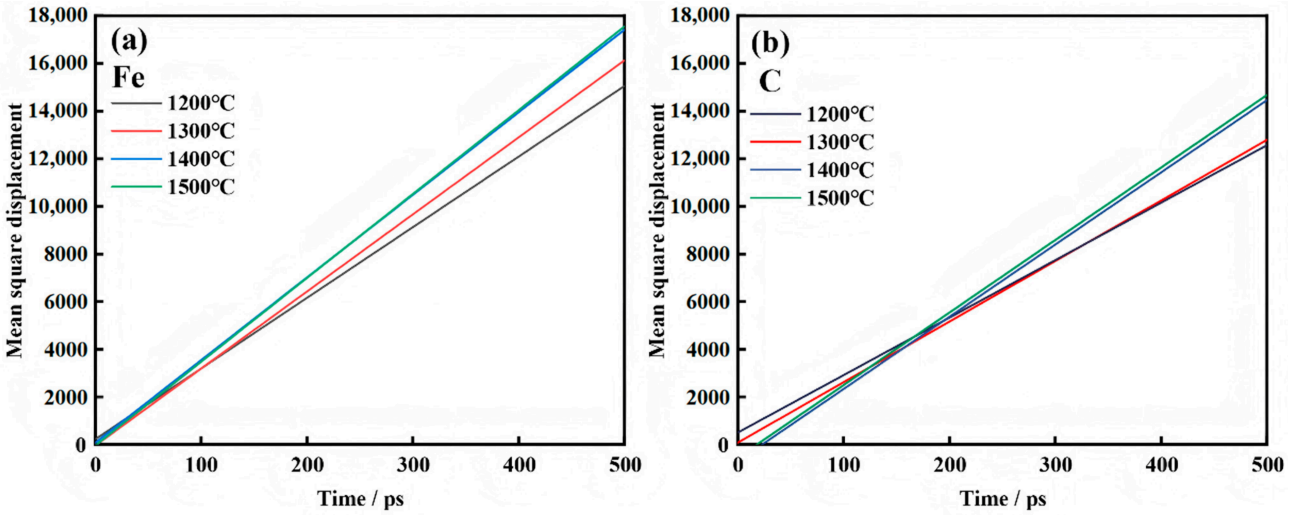


Figure 7. Effect of temperature on the mean square displacements (MSDs) of Fe and C atoms. (**a**) MSD curves for Fe atoms; (**b**) MSD curves for C atoms.

To qualitatively illustrate the dynamic evolution of representative local structures, snapshots of Fe–V, Fe–C, V–C, and Fe–V–C configurations were extracted over 0–100 ps, as shown in Figure 8. These snapshots were used to visualize the local dissociation, reassociation, and structural reorganization occurring in the high-temperature melt [27–29]. All types of clusters underwent continuous dissociation, diffusion, and reassociation, indicating the existence of a dynamic equilibrium in the high-temperature melt. The iron-vanadium configuration gradually dispersed over time, resulting in relatively poor structural stability. Although some Fe–C bonds were broken, the released Fe and C atoms reassociated at other locations, and Fe–C connections remained observable throughout the simulation. V–C units also dissociated and reformed but persisted at each sampled time, indicating a strong local V–C association consistent with the RDF and coordination-number results.

Compared with binary clusters, multicomponent Fe–V–C clusters exhibited more complex connectivity. During dynamic equilibration, Fe–V–C clusters partially dissociated into Fe–C, V–C, and Fe–V coordination units, which subsequently recombined with nearby atoms to form new Fe–V–C clusters [30]. Relatively persistent V–C units acted as local connections to surrounding Fe atoms and Fe–C units, favoring the formation of complex Fe–V–C clusters. This dynamic association increased local structural complexity and constrained the migration of Fe and C, providing an atomic-scale explanation for the lower fluidity and higher viscosity of vanadium-containing hot metal [31].

Based on these results, an atomic structural model for cluster formation in vanadium-containing hot metal was developed (Figure 9). Fe, V, and C atoms formed basic Fe–V, Fe–C, and V–C coordination units, with V and C serving as local coordination centers linked to surrounding Fe atoms. Increasing the vanadium content increased the population of V–C units, which connect and aggregate with nearby Fe atoms and Fe–C units to form increasingly complex multicomponent Fe–V–C clusters. The resulting increase in local structural order and connectivity raised the resistance to atomic diffusion and migration, thereby reducing hot metal fluidity and increasing viscosity.

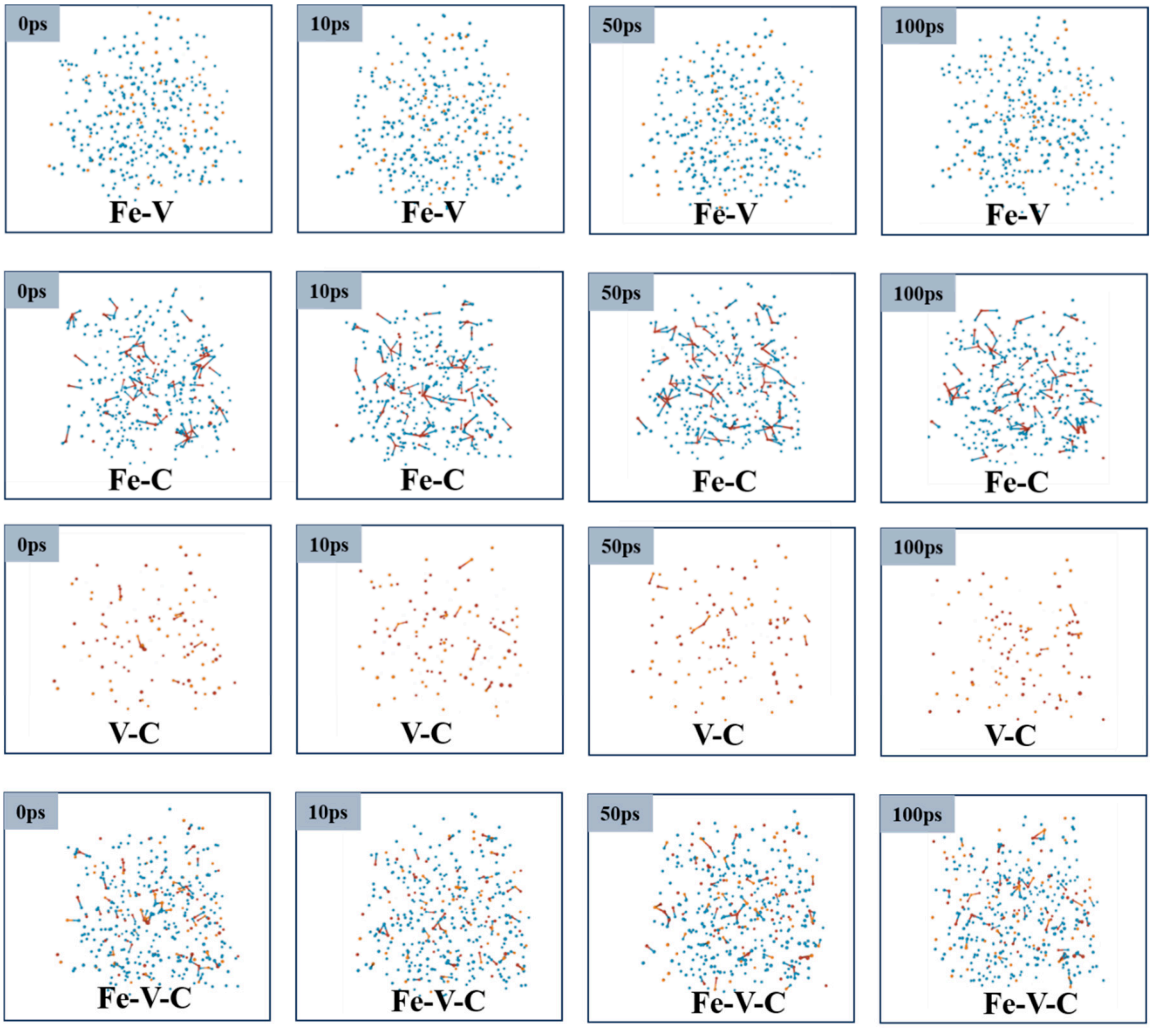


Figure 8. Dynamic evolution of different atomic clusters in vanadium-containing hot metal. Blue spheres represent Fe atoms, orange spheres represent V atoms, and red spheres represent C atoms.

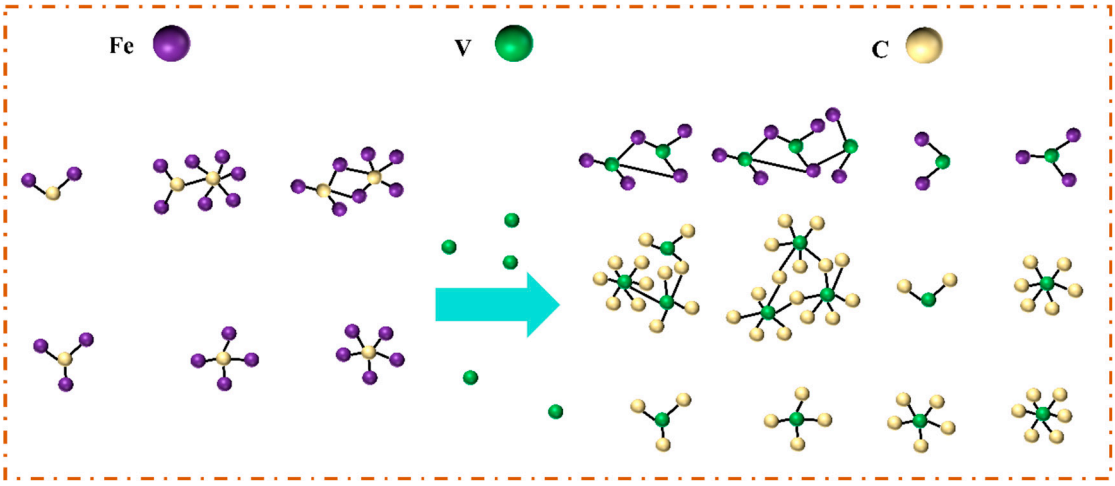


Figure 9. Atomic structure model and cluster structure formation process of hot metal.

4. Conclusions

(1) Hot metal viscosity and characteristic melting temperature increased with vanadium content. Below 0.30 wt.% V, viscosity remained relatively low and showed weaker

temperature dependence. At 0.30 wt.% V and above, viscosity increased, fluidity deteriorated, and temperature dependence became more pronounced.

(2) At 1500 °C, increasing the vanadium content from 0.10 to 0.50 wt.% raised the average V–C coordination number from 7.780 to 8.218, while decreasing the C–Fe and Fe–C coordination numbers from 4.565 and 0.980 to 3.965 and 0.930, respectively. Thus, increasing vanadium promoted V–C cluster formation and redistributed the local environment of C from Fe–C coordination toward V–C coordination.

(3) The MSDs and corresponding slopes of Fe and C decreased with increasing vanadium content, indicating suppressed atomic mobility, particularly for C. Increasing temperature enhanced Fe and C mobility while weakening Fe–C coordination and short-range order in the melt.

(4) V–C units repeatedly dissociated and recombined and connected with Fe–C and Fe–V units to form complex multicomponent Fe–V–C clusters. These clusters increased local structural order and connectivity, restricted Fe and C mobility, and thereby contributed to the increase in hot metal viscosity.

Author Contributions: Conceptualization, J.C., P.G., Z.P., D.W., X.X. and S.R.; methodology, J.C., Y.P., P.G., X.L., Z.S. and D.W.; software, J.C., Y.P., X.L. and Z.S.; validation, J.C., Y.P., X.L. and Z.S.; formal analysis, J.C., Y.P., X.L. and Z.S.; investigation, J.C., Y.P., X.L. and Z.S.; resources, P.G., Z.P., D.W., X.X. and S.R.; data curation, J.C., Y.P., X.L. and Z.S.; writing—original draft preparation, J.C., Y.P., X.L. and Z.S.; writing—review and editing, J.C., Y.P., P.G., X.L., Z.S., Z.P., D.W., X.X. and S.R.; visualization, J.C., Y.P. and X.L.; supervision, P.G., Z.P., D.W., X.X. and S.R.; project administration, P.G., X.L., Z.P., D.W., X.X. and S.R.; funding acquisition, P.G., D.W. and X.X. All authors have read and agreed to the published version of the manuscript.

Funding: This work was financially supported by the National Natural Science Foundation of China (52504370), the Guiding Funds of the Central Government for Supporting the Development of Local Science and Technology (24ZYQB003), Scientific Research Plan Project of Education Department of Shaanxi Provincial Government (25JC056), and the State Key Laboratory of Metal Forming Technology and Heavy Equipment (B2408100.W18).

Data Availability Statement: The original contributions presented in this study are included in the article. Further inquiries can be directed to the corresponding authors.

Acknowledgments: We thank Ning Qiu of Xi'an University of Architecture and Technology for assistance with surface analysis and Raman spectroscopy measurements at the Instrument Analysis Center.

Conflicts of Interest: The authors declare no conflicts of interest.

References

1. Zhu, F.; Ma, Z.; Gao, G.; Qiu, K.; Peng, W. Process Mineralogy of Vanadium Titanomagnetite Ore in Panzhihua, China. *Separations* **2023**, *10*, 147. [CrossRef]
2. Wu, J.X.; Sun, H.W.; Chen, F.W.; Wang, Y.J.; Liu, Z.Y.; Lai, Z.T. A new vanadium-titanium magnetite deposit containing 358 million tonnes discovered in Weiya, Hami, Xinjiang. *Geol. China* **2025**, *52*, 1904.
3. Li, L.J.; Zhang, C.D.; Liu, Y.; Zhao, S.X.; Zhao, J.Q.; Xu, K. Research progress on non-blast-furnace smelting of vanadium-titanium magnetite and comprehensive utilization of titanium slag. *China Metall.* **2025**, *35*, 44.
4. Shen, Z.H.; Xing, X.D.; She, Y.; Li, X.Y.; Miao, H.S.; Guo, P.H. Viscous flow characteristics and molecular dynamics simulation of titanium-containing hot metal. *J. Iron Steel Res.* **2025**, *37*, 845.
5. Jiang, Z.; Yu, W.; Song, L.; Hou, P.; Hu, M.; Bai, C. Influencing mechanism of (V, Ti)@(C, N) compounds on the viscosity of hot metal. *Ironmak. Steelmak.* **2024**, *51*, 397. [CrossRef]
6. Hou, P.; Yu, W.Z.; Bai, C.G.; Pan, C.; Yuan, W.N.; Li, T. Viscous flow properties and influencing factors of hot metal from vanadium-titanium magnetite smelting. *Iron Steel* **2022**, *57*, 57.
7. Gao, S.; Jiao, K.; Zhang, J.; Fan, X.; Liu, Z.; Zheng, A. Review on the viscosity of iron-based melts in metallurgical process. *ISIJ Int.* **2022**, *62*, 2172. [CrossRef]

8. Teng, X.Y.; Liu, H.L.; Wang, H.R.; Shi, Z.Q.; Ye, Y.F.; Geng, H.R. Liquid structure and viscosity of Fe–C eutectic alloy. *J. Iron Steel Res.* **2002**, *14*, 5.
9. He, Y.Y.; Liu, Q.C.; Yang, J.; Yang, B.N.; Long, M.H.; Zheng, H.M.; Liu, C.W.; Wei, M.X. Study on the fluidity of titanium-containing hot metal. *Iron Steel Vanadium Titan.* **2010**, *31*, 10.
10. Wen, G.; Yan, Y.; Zhao, S.; Huang, J.; Jiang, G.; Yang, X. Study on the properties of vanadium- and titanium-containing hot metal. *Iron Steel* **1996**, *31*, 6.
11. Deng, Y.; Zhang, J.L.; Jiao, K.X. Viscosity measurement and prediction model of molten iron. *Ironmak. Steelmak.* **2018**, *45*, 773. [CrossRef]
12. Zhang, Q.; Wang, J.; Tang, S.; Wang, Y.; Li, J.; Zhou, W.; Wang, Z. Molecular dynamics investigation of the local structure in iron melts and its role in crystal nucleation during rapid solidification. *Phys. Chem. Chem. Phys.* **2019**, *21*, 4122. [CrossRef] [PubMed]
13. Li, J.; Xiao, R.; Qin, J.; Ruan, Y.; Li, H. The structural exploration of thermodynamics and dynamics in Ti-Ni liquid by ab initio molecular dynamics simulation. *Comput. Mater. Sci.* **2023**, *230*, 112499. [CrossRef]
14. Yan, H.J.; Liu, L.; Zhuang, J.C.; Zhou, P.; Zhou, C.Q. Molecular dynamics simulation of carbon effect on the thermal physical properties of the molten iron. *ISIJ Int.* **2019**, *59*, 221. [CrossRef]
15. Hepburn, D.J.; Ackland, G.J. Metallic-covalent interatomic potential for carbon in iron. *Phys. Rev. B* **2008**, *78*, 165115. [CrossRef]
16. Diao, J.; Liu, L.; Gu, W.; Gu, P.; Wang, G.; Xie, B. Investigation on viscosity and melting temperature of vanadium, titanium, chromium containing hot metal. *Steel Res. Int.* **2019**, *90*, 1900069. [CrossRef]
17. Yang, H.; Liu, Y.; Wan, X.; Zhang, T.; Lin, S.; Wang, K.; Li, X. Microstructure and Mineral Phase Evolution of Vanadium Slag by Modulating the CaO/V_2O_5 Ratio. *Minerals* **2023**, *13*, 628. [CrossRef]
18. Jiang, C.; Li, K.; Zhang, J.; Sun, M.; Bi, Z. Structural characteristics of liquid iron with various carbon contents based on atomic simulation. *J. Mol. Liq.* **2021**, *342*, 116957. [CrossRef]
19. Zhang, Y.; Jiao, K.; Zhang, J.; Fan, X.; Gao, S. Viscosity and structure correlation mechanism of Fe–Cr–C melt based on MD simulation. *J. Mol. Liq.* **2024**, *413*, 125903. [CrossRef]
20. Gao, S.; Jiao, K.; Zhang, J.; Fan, X.; Zong, Y. Association of atomic clusters and free volume with the viscosity of Fe–C melts. *Chem. Phys. Lett.* **2022**, *806*, 139983. [CrossRef]
21. Belashchenko, D.K.; Mirzoev, A.; Ostrovski, O. Molecular dynamics modelling of liquid Fe–C alloys. *High Temp. Mater. Process.* **2011**, *30*, 297. [CrossRef]
22. Posner, E.S.; Steinle-Neumann, G. Compositional effects in the liquid Fe-Ni-C system at high pressure. *Phys. Chem. Miner.* **2022**, *49*, 43. [CrossRef]
23. Luo, C.; Min, Y.; Guo, P.; Chen, F.; Jiao, S.; Liu, C. Molecular dynamics simulation of the structure and transport properties of Fe–Cr–Ni alloy melts. *J. Non-Cryst. Solids* **2025**, *650*, 123362. [CrossRef]
24. Lü, Y.; Cheng, H.; Chen, M. A molecular dynamics examination of the relationship between self-diffusion and viscosity in liquid metals. *J. Chem. Phys.* **2012**, *136*, 214505. [CrossRef] [PubMed]
25. Das, S.K.; Horbach, J.; Koza, M.M.; Mavila Chatoth, S.; Meyer, A. Influence of chemical short-range order on atomic diffusion in Al-Ni melts. *Appl. Phys. Lett.* **2005**, *86*, 011918. [CrossRef]
26. Jiang, C.; Liu, B.; Liang, W.; Zhang, J.; Li, K. Microstructure evolution and properties of liquid Fe–P with different phosphorus content: Molecular dynamic investigation. *J. Mol. Model.* **2025**, *31*, 137. [CrossRef] [PubMed]
27. Pan, S.; Feng, S.; Qiao, J.; Dong, B.; Qin, J. The atomic structure of liquid Fe–C alloys. *J. Alloys Compd.* **2015**, *648*, 178. [CrossRef]
28. Feng, G.; Jiao, K.; Zhang, J.; Gao, S. High-temperature viscosity of iron-carbon melts based on liquid structure: The effect of carbon content and temperature. *J. Mol. Liq.* **2021**, *330*, 115603. [CrossRef]
29. Fan, X.; Gao, S.; Zhang, J.; Jiao, K. Analysis of the structure and viscosity of iron melts containing titanium at various concentration. *J. Mol. Liq.* **2023**, *386*, 122519. [CrossRef]
30. Fan, X.; Huang, Y.; Han, J.; Gao, S.; Zhang, J.; Jiao, K.; Chen, Z. Viscosity and structure studies of iron-based quaternary melts: The effect of S. *Met. Mater. Int.* **2024**, *30*, 1783. [CrossRef]
31. Pan, S.P.; Feng, S.D.; Qiao, J.W.; Wang, W.M.; Qin, J.Y. Correlation between local structure and dynamic heterogeneity in a metallic glass-forming liquid. *J. Alloys Compd.* **2016**, *664*, 65. [CrossRef]

Disclaimer/Publisher's Note: The statements, opinions and data contained in all publications are solely those of the individual author(s) and contributor(s) and not of MDPI and/or the editor(s). MDPI and/or the editor(s) disclaim responsibility for any injury to people or property resulting from any ideas, methods, instructions or products referred to in the content.